Current Limiting Schemes and their Stability Implications for Blackstart of Power Systems with Inverter-Based Resources

José R. Martínez*‡, Olga Lavrova*, Satish Ranade*

* Klipsch School of Electrical and Computer Engineering, New Mexico State University, Las Cruces, NM, USA

(jrm10020@nmsu.edu, olavrova@nmsu.edu, sranade@nmsu.edu)

‡ Corresponding Author; José R. Martínez, New Mexico State University, Las Cruces, NM, USA, Tel: +1 575 571 9216, jrm10020@nmsu.edu

Received: 13.07.2024 Accepted:19.08.2024

Abstract- This paper analyzes two different current limit schemes within IBRs, focusing on their effectiveness and addressing performance deficiencies where identified. The context of this analysis is an islanded blackstart scenario, utilizing the IEEE-13 node test feeder augmented with an induction motor. MATLAB Simulink™ serves as the primary simulation platform. This study aims to contribute to the robust and efficient operation of modern power grids by refining the simulation accuracy of IBR behaviors through means of additional implementation of voltage setpoint and current limit control schemes. The main contribution from this paper is that it provides steps to achieve a successful dynamic response, blackstart, and current limit response from the amended detailed current limit scheme presented in this paper, which is inspired by current limit schemes found in existing literature. This involves providing novel solutions that turned the initially unstable system response to a stable one, while still providing current limitation capability.

Keywords: Reliability, Resiliency, Blackstart, Induction Motor, IBR, Stability

1. Introduction

Inverter-based resources (IBRs) are increasingly gaining popularity and being commercially implemented in modern power systems, making the IBR capabilities that can enhance grid functionality more and more essential. One of these capabilities is the ability to initiate power restoration in islanded conditions, known as blackstart. If a segment of a power system is outaged, and one or more IBRs are able to dispatch power faster than a conventional power generation unit, the IBR can poten- tially provide the ability to initiate power restoration in the island. However, to perform or assist with blackstart, the IBR must be capable of what is referred to as grid- forming capabilities, that is, the ability for the IBR to provide the dynamic response [1], frequency regulation, and reactive capability. One significant difference in IBRs compared to conventional units is that IBRs are limited in the amount of current which they can provide (inject). Due to physical device limitations IBRs can only inject on the order of approximately 1.5 p.u. (per unit) rated current, whereas a conventional unit can deliver up to 6 p.u. current during short periods of time [2]. These factors restrict the extent to which an IBR may offer reactive support and poses a significant obstacle to IBR blackstart [1]. As late 2023, only five real life grid forming IBR's are currently in operation in the US [3], and as such, most of the knowledge and research of grid-forming IBR's are known from computer simulation. When analyzing grid-forming IBRs using simulation software like MATLAB Simulink™, GE PSLF™, Siemens PSSE™, or PSCAD™, it is important to have an appropriate current-limiting model for an IBR. This ensures that the IBR models may then be accurately used for interconnection study criteria established by reliability coordinators; an example of such criteria may be

found in [4]. Various IBR manufacturers have developed their own proprietary models for their respective IBRs, as there is no universally standardized or detailed open-source model approach for modelling the current limitations of an IBR. Hence, the objective of this paper are three-fold: (1) to investigate several present current-limiting models of grid-forming IBRs; (2) apply the detailed model to a blackstart condition of an IEEE- 13 test system [2]; and (3) to suggest novel modifications towards improving stability.

The current limiting scheme is often the key factor in the use of IBRs as grid forming sources (GFM) in conventional distribution systems [5]. The GFM must handle transient loads such as motor starts [6], and such duties can be severe during blackstart. In this paper, the current limiting schemes inspired by [5], [7], and [8] are examined.

1.1 Goals of Paper

The stability of these schemes, given a set of assumptions and study methodology, is analyzed. The main contributions to GFM blackstart this paper aims to provide are the following:

1) Make simplified and complete versions of the current limiting scheme shown in [5], [7], and [8], and assess their stability and current limit capability. Successful results will be both (a) stable and (b) current limited according to a specific current setpoint. Results will indicate lack of success given this criteria.
2) Provide novel solutions that contribute to the restoration of stable, current limited conditions.

After study is presented, the conclusion section provides a list of contributions tailored to actual study findings.

1.2 Note on Models Implemented

This section brings an integral point to the attention of the reader in terms of models used. Modeling techniques for this study are purposefully simplistic in nature. This, however, does not take merit away from the results, since finding a possible instability using simplistic modeling means that instability can occur with more advanced models, as more advanced models built on the same core fundamentals the simplistic modeling in this paper capture. The models will be described in detail throughout the length of this paper.

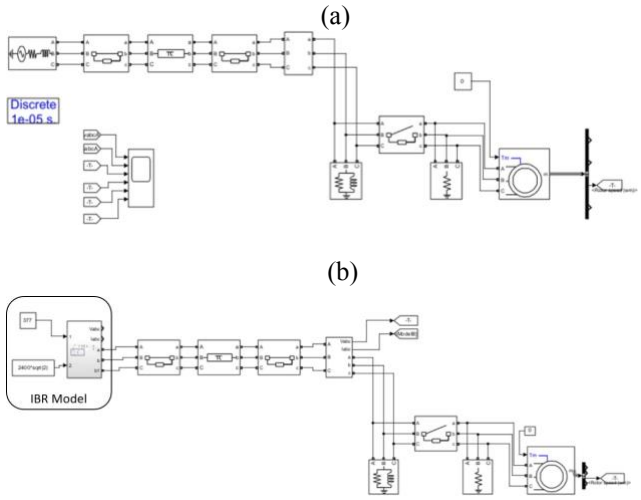

Fig. 1. Template Simulink^{TM} models with (a) ideal source, and (b) baseline IBR source.

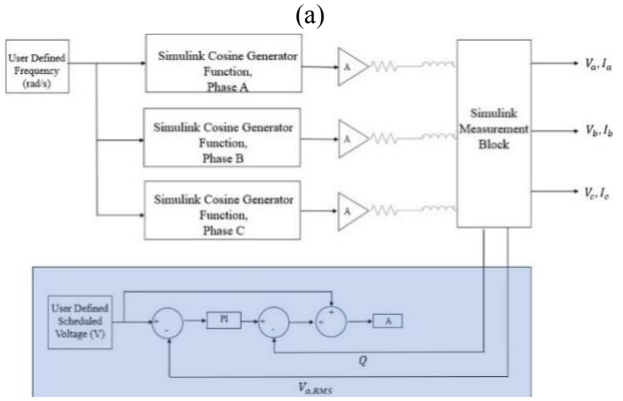

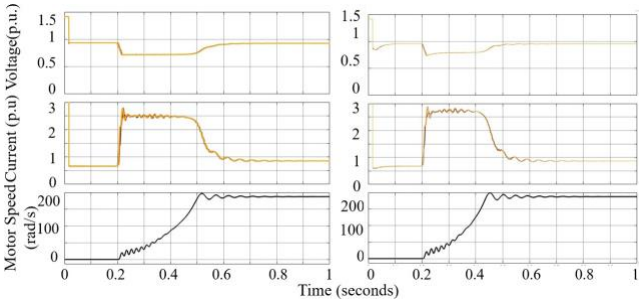

Fig. 2. (a) Block diagram showing logic for the IBR droop control scheme, and (b) output results comparing motor start using ideal source and IBR source. Ideal source plots in left, and IBR plots on right

2. Methodology

This study follows the outline below:

1) Develop a baseline IBR Model in Simulink™, and validate the model's performance as compared to the conventional generator.
2) Use the developed IBR model as a source within an IEEE-13 test system to investigate blackstart capability.
3) Develop simplified and detailed current limiting schemes within the IBR model. Then compare the performance of these models during the blackstart scenario.
4) Develop a theoretical model verifying behavior observed during the modeling process.

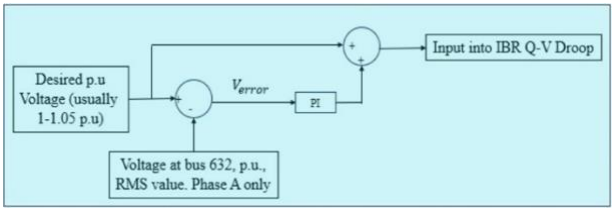

Fig. 3. Automatic voltage setpoint control scheme.

2.1 Baseline IBR Model

Fig. 1 shows the template Simulink™ models developed to validate the performance of the baseline IBR model. The model shown in Fig. 1(a) assumes an ideal conventional generator supplying the system with motor blackstart at 0.2 seconds. The second model, shown in Fig. 1(b) blackstarts the same induction motor, but replaces the ideal generator with an IBR unit equipped with QV droop.

Fig. 2 shows the details of implementation of the IBR droop controller; this implementation is inspired by [9-14]. This controller takes as inputs the IBR output V_{rms} and reactive power Q values, and outputs a new voltage amplitude. Note, V_{ideal} is the output of the QV droop scheme, it is depicted as the variable 'A' in the shaded box of Fig. 2(a); A is then fed as a scale factor to the amplitude of the IBR.

$$V_{ideal} = V_{set} + (\text{PI control})(V_{set} - V_{act}) - V_{droop}\,Q \quad (1)$$

where:

- V_{ideal} is the output voltage from the QV droop control, an ideal source voltage magnitude (shown as 'A' in the shaded box of Fig. 2(a), then fed as a scale factor to the IBR voltage amplitude)
- V_{set} is a desired user defined voltage setpoint
- V_{act} is the actual output voltage from the IBR terminals
- V_{droop} is the droop slope multiplier
- Q is the actual output reactive power from the IBR terminals

Fig. 2(c) shows the side-by-side comparison of the ideal source and the baseline IBR source blackstarting the induction motor at 0.2 seconds. The basic IBR model has a successful dynamic response, nearly identical to the ideal source. Note that neither of the models have any current limitations yet, current limitation schemes will now be added to the IBR model in the following sections.

2.2 Automatic Voltage Setpoint Control Model

In order for the IBR to be capable of blackstarting the system, it would be desirable to control voltage at a bus physically farther away from the generator terminals that can dynamically adjust the IBR according to system needs. In this way, the IBR can provide voltage support at a closer point to where load is being blackstarted, and thus be better able to maintain voltages within nominal operating values. Based on these needs and with inspiration from [15], an additional control scheme would be needed to implement this capability to the system studied. Fig. 3 shows such an additional controller developed for the IBR model: The controller takes the Bus 632 voltage and uses a PI controller in a feedforward fashion to keep Bus 632 voltage regulated at 1 p.u. The output of this control scheme acts as input to the QV droop scheme.

2.3 Modified IEEE System Model

The performance of the IBR model developed in the previous section will now be tested in the modified IEEE-13 test system, shown in Fig. 4. IEEE-13 will be considered as an island that the grid-forming IBR must initiate the process of blackstarting. The grid-tie (normally at bus 650) is deleted, and in its place, the IBR model will be used to blackstart the island. In addition, the induction motor (IM) load is moved to bus 680. This presents a more difficult scenario for blackstarting the induction motor load when the circuit-miles distance between the motor and the power source is greater, as compared to leaving the IM at its original location [16]. The loads in the modified test system are kept as constant power loads, and all other parameters of the IEEE-13 test system are kept the same as in [17]. Note that Simulink™ converts these to constant impedance loads. The induction motor parameters as input into Simulink™ are listed below. Note that the size of the induction motor is immaterial to the study results, as the IBR model used adjusts the output to meet system demands. Once current limitation is applied to the IBR model, this motor will allow

to showcase current limiting ability of schemes through potential limitation of motor inrush current.

- Nominal Power: 10 kVA
- Voltage (line-to-line): 4160 V
- Frequency: 60 Hz
- Stator Resistance: 0.3 Ohm
- Stator Inductance: 0.0053 H
- Rotor Resistance: 0.23 Ohm
- Rotor Inductance: 0.0027 H
- Mutual Inductance: 2.65 H
- Inertia: 2 J
- Friction Factor: 10 N.m.s
- Pole pairs: 2

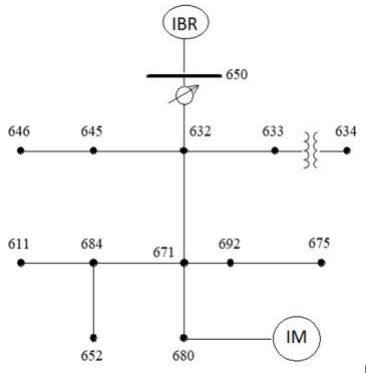

Fig. 4. Modified IEEE-13 Bus System used for this study.

(a)

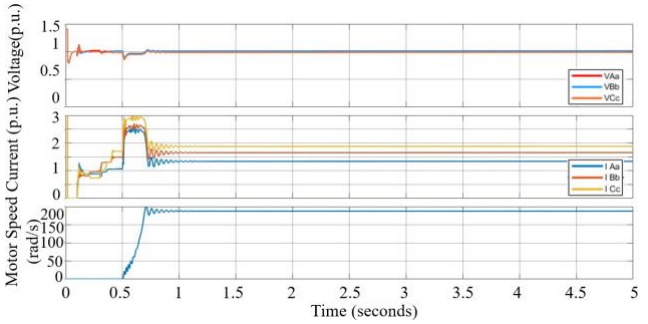

(b)

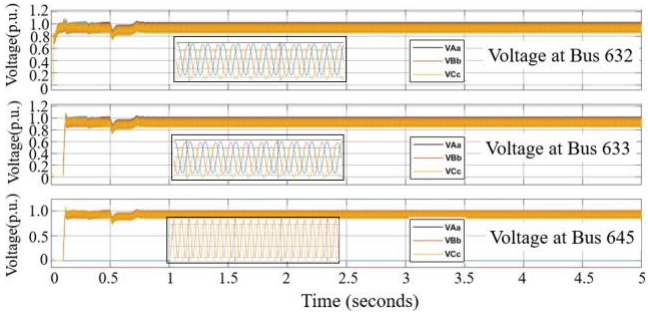

Fig. 5. (a) Model B Source output and Motor speed in response to blackstart; (b) Select IEEE-13 bus voltage waveforms.

2.4 Blackstart Sequence and Base Case Results

Metrics for determining whether the system was stable or not are the following [18]:

- Per unit voltage waveforms damp out after breaker(s) close(s) within a reasonable amount of time to a reasonable value (Ideally 0.95 p.u. to 1.05 p.u).
- Voltage waveforms remain damped, and their final (settled) values (in p.u.) are evaluated after a 5 second run.

Note that there exist many combinations and permutations of possible blackstart sequences. From a mathematical perspective, if the IEEE-13 bus plus induction motor loads are linearized around an operating point of 2400 V and some base output current, each blackstarted load will cause some perturbation, assume this perturbation to be ϵ. In a linearized system, superposition principles apply and makes it so that ϵ_i, may be presented in different orders and yield the same overall perturbation to the blackstarting system, but may result in nonlinear results from a stability standpoint [19].

Given this, combined with the fact that the cranking path must physically make sense in terms of a real world application [20], of the many blackstart permutations and combinations, the cranking path listed in Table 1 is chosen.

Table 1. Blackstart Sequence of IEEE-13 plus Induction Motor

Time (seconds)	Bus Number Load Blackstarted
0.1	632 and 645
0.15	633 and 634
0.2	646
0.25	671 (load on line 671-632)
0.3	671 (load on line 671-675)
0.35	692 and 675
0.4	684, 611, and 652
0.5	680 (induction motor load

Fig. 5 shows the results of the system response throughout the blackstart of IEEE-13 plus induction motor, as well as voltage plots for selected IEEE-13 buses. The results of this base case show that stability was achieved after blackstarting the entire IEEE-13 plus induction motor. This case can now act as the base case for the development and investigation of the current limit schemes - which are the primary focus of this paper.

3. Current Limiting Scheme Development for IBR Model

3.1 Simplified Current Limiting Scheme

The first approach to a current limit scheme will be to develop a simplified scheme which only focuses on a current loop to limit current. To design such a solution, it is important to first derive equations for a complete current scheme, for which references [5], [7], and [8] were instrumental.

The per-phase source voltage for a 3-phase IBR (see Fig. 1) can be expressed as:

$$e_a = Ri_a + L\frac{di_a}{dt} + v_a \tag{2}$$

where:

- e_a is the internal voltage supplied by the IBR
- R is the IBRs internal resistance
- L is IBRs internal inductance
- i_a is the IBRs output phase A current
- v_a is the IBR's output phase A terminal voltage supplied to grid

Note, similar equations apply for phases b and c. Using the Park's transformation [21-23], equation (2) can be translated to the dq0 synchronous reference frame to arrive to the equations (3) and (4). Note that the zero sequence component of the transform is not listed or used for the purposes of this paper:

$$e_d = Ri_d + L\frac{di_d}{dt} - \omega Li_q + v_d \tag{3}$$

$$e_q = Ri_q + L\frac{di_q}{dt} + \omega Li_d + v_q \tag{4}$$

Denoting Laplace transforms of the voltage and current with corresponding upper case letters, the above equations can be written in the Laplace domain as equations (5) and (6).

$$E_d = (R + sL)I_d + V_d - \omega LI_q \tag{5}$$

$$E_q = (R + sL)I_q + V_q + \omega LI_d \tag{6}$$

Where ω is the IBR frequency in rad/s.

Thus, Ed and Eq can be controlled to limit the current. A common method to enforce the current limit is to use PI controllers, as shown in Fig. 6, to drive the errors between d and q axis currents and the corresponding limits to zero; this is shown in [5], [7], and [8]. Suitable combinations of terms in equations 5 and 6 can be used as feed-forward signals. Fig. 6 shows the terms $V_d + \omega LI_q$ and $V_q + \omega LI_d$ as feed-forwards. The current-limited values of Ed and Eq can now be written as

$$E_{d,limit} = (PI)I_{err,d} + V_d - \omega LI_{err,q} \tag{7}$$

$$E_{q,limit} = (PI)I_{err,q} + V_q + \omega LI_{err,d} \tag{8}$$

(a)

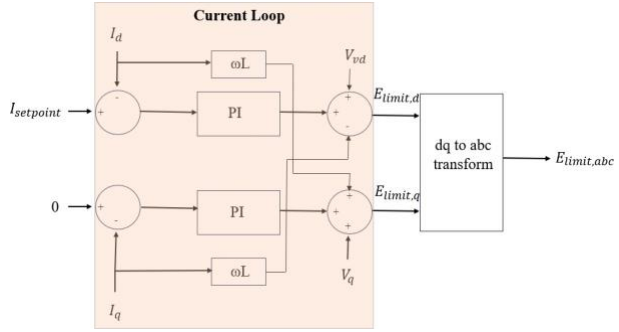

(b)

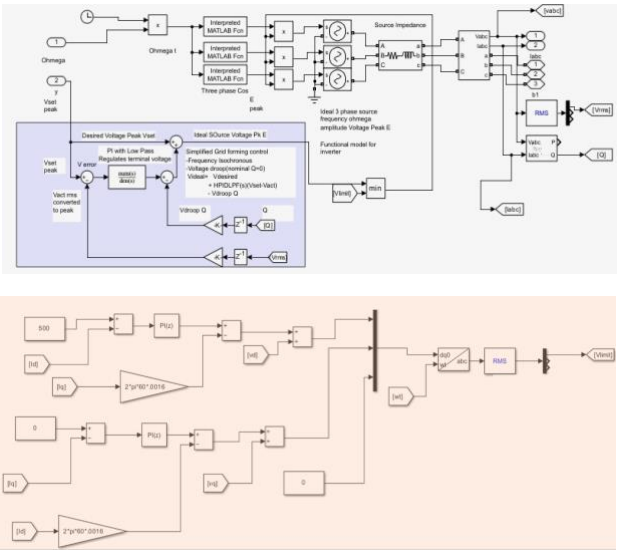

Fig. 6. (a) Simplified current limit scheme schematic (b) Simulink™ implementation.

Where,

$$I_{err,d} = I_{setpoint,d} - I_d \tag{9}$$

$$I_{err,q} = I_{setpoint,q} - I_q \tag{10}$$

Fig. 6(b) shows the Simulink™ implementation of this simplified scheme, color-coded in peach color. Equations (11) and (12) provide initial guess values for the PI controller gain

values of this scheme, as described in [24].

$$\sqrt{L2 * C} = \sqrt{\frac{.0016}{2} * 15.04e-6} = .00011\ sec \quad (11)$$

$$k_p = \frac{L1}{t} = \frac{.0016}{2*.00011} = 7.27, k_i = \frac{L1*R1}{t} = 0.727 \quad (12)$$

where

- t represents a time constant associated with resonant frequency
- k_p is the proportional gain
- k_i is the proportional gain

The current setpoint was set to 500A (1.8 p.u.), a limit significantly below the system current demand. Results are shown in Fig. 7. For the bulk of this response, the output current has been successfully limited to within the1.8 p.u. limit. Note that the induction motor was able to be blackstarted successfully.

The oscillations in the output waveforms seems to be driven by the induction motor behavior, since all the system's bus voltages oscillate up and down in tandem with motor speed oscillation - as illustrated in the current and motor speed graphs in Fig. 7. The induction motor is able to draw its entire inrush current even though the current limiter is in place. Therefore, this oscillatory behavior could be due to the fact that the current limit control is conflicting with the automatic voltage setpoint control that feeds into the unit.

To confirm that this is the case, a separate simulation was performed where the voltage setpoint control was disabled. Results displayed in Fig. 8 show that there is decreased oscillation, confirming that, indeed, there was a conflict in controls for this simplified scheme. To resolve this conflict, we have developed a more advanced current limiting scheme, described in the next section.

3.2 Modified Current Limiting Scheme

A more advanced current-limiting scheme was developed by adding a voltage control loop to the current control loop, adding logic for the scheme to decide whether signals are above or below a current setpoint, and feeding into this combined scheme the Q-V droop output, as illustrated in [25]. This approach was inspired by [5], [7], and [25]. Fig. 9 displays the block diagram of the detailed scheme, as well as the Simulink™ implementation.

3.3 Detailed Simulink™ Model Initial Run and Signal Decision Description

The advanced current-limiting scheme has a signal decision that takes the voltage loop's output signals; the working of this signal decision will now be described; this approach is inspired by, but not identical to, reference [5].

Consistent with reference [5], the present target value is determined within the "if" phrase. If the magnitude of the dq output, which is calculated as the square root of the sum of the squares, is smaller than the setpoint, then there is no need to adjust the currents. If the magnitude of the d and q combined output exceeds the setpoint, then the q component serving as input into the current loop

(a)

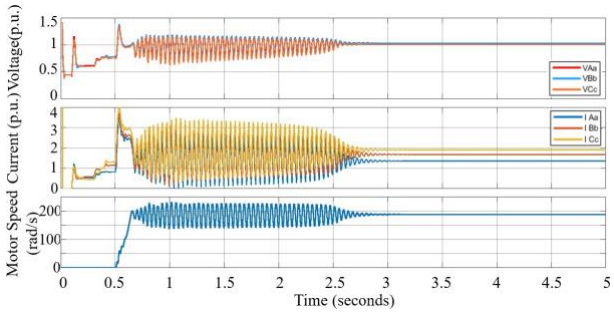

(b)

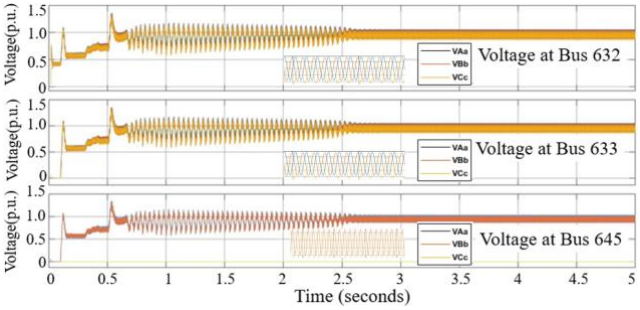

Fig. 7. (a) Output voltage, current, and motor speed output and (b) Select IEEE-13 bus voltages in response to simplified current limit scheme.

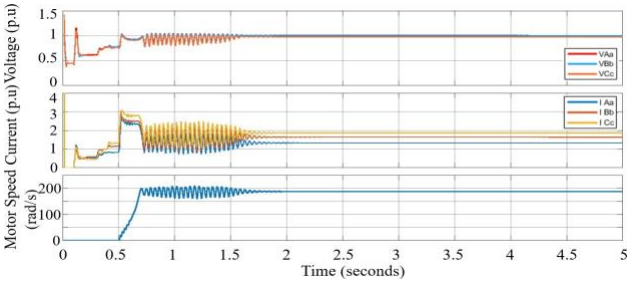

Fig. 8. Output voltage, current, and motor speed output, Model B working with simple current limit scheme, but with automatic voltage setpoint scheme disabled.

should be set to zero while keeping the d component unaltered. It should be noted that the bottom part of the voltage scheme, which calculates the q component of the voltage controller, could not be captured owing to constraints in fig. size. However, this calculation is similar

to the "d" component calculation.

The scheme was tested with a both a 1000 A (3.6 p.u.) current setpoint (normal operating conditions) and a 500 A (1.8 p.u.) current setpoint (current clipping should be noticeable at the 500 A (1.8 p.u) current setpoint level). Fig. 10 shows a successful experiment in terms of current limit: the 500 A (1.8 p.u.) setpoint example clearly shows a delayed motor start and significantly reduced current output when compared to the 1000 A (3.6 p.u.) current setpoint output. Furthermore, the 1000 A (3.6 p.u.) case current output looks very similar to that of the 500 A case, so there is no current clipping capability in the complete current scheme as is.

However, it is still clearly observable from Fig. 10 that there is a voltage instability in both the 1000 A (3.6 p.u.) and 500 A (1.8 p.u.) limit scenarios. Typically, reducing the instability can be achieved by lowering the integral gain of the current controller's four PI controllers. This flattens the initial voltage response and provides optimal stability. However, the 500 A (1.8 p.u.) current setpoint is no longer limiting the current as well as it did before. Decreasing the setpoint to 400 A did not make a difference in the response; this is shown in Fig. 10. This unstable behavior was verified in an extended 30 second run.

This serves as an instance of instability in a scenario where stable output is expected. Given that lowering integral gain jeopardizes the current limiting ability of the current limit scheme, a novel approach needs to be implemented to retain both stability and current clipping. Section 3.4 explores such an implementation.

3.4 Novel Switched Proportional Gain Scheme

A novel automatically stepped control via proportional gain actualization is proposed. This additional control will assume a zero integral gain.

The progressive gain control can be tailored to any system, with as many proportional gain 'taps' as the user desires, as well as tailored to the user's desired setpoints in voltage and current. Note that the P values for the switch are not universal across all desired current limit scenarios. Once a desired setpoint is known, appropriate experimentation and tuning has to be done on the scheme to find optimal switched P values.

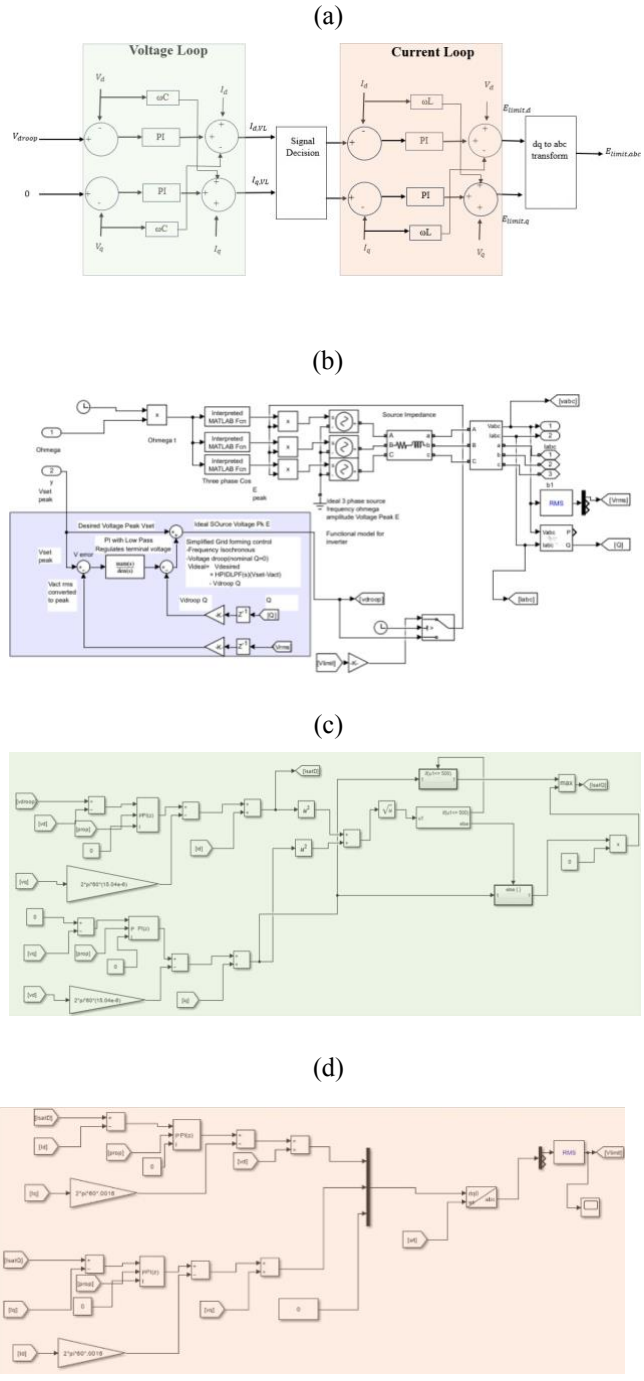

Fig. 9. Complete Model B IBR current limit scheme, showing (a) schematic, (b) Simulink^{TM} Model B IBR modified loopback, (c) voltage loop and (d) current loop.

(a)

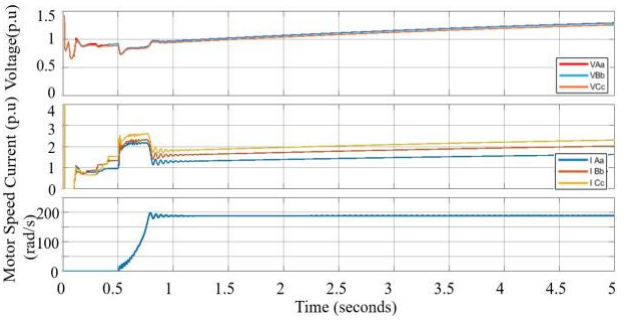

(b)

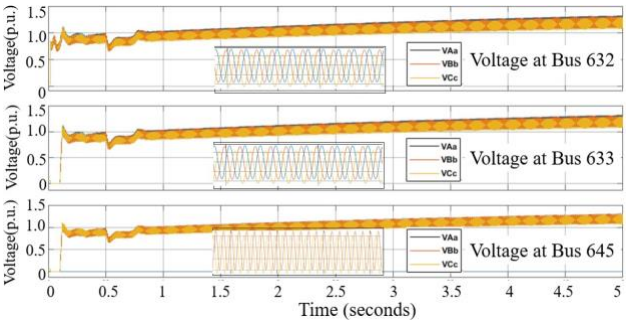

(c)

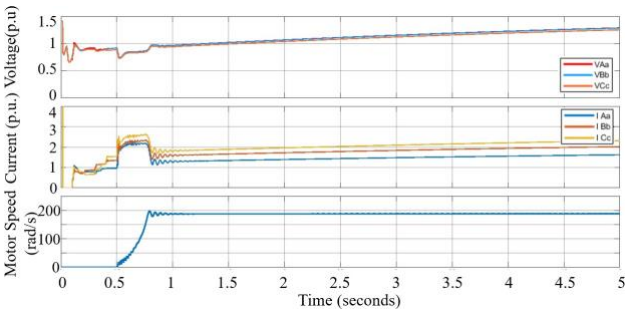

(d)

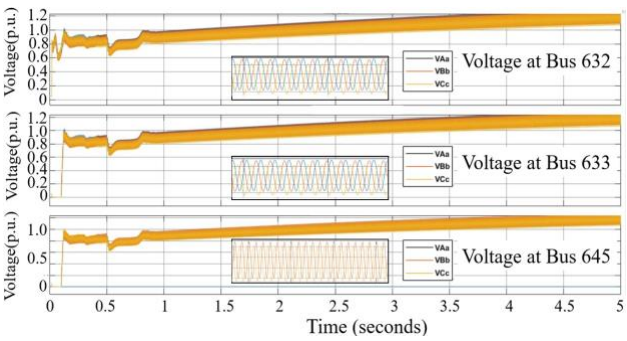

Fig. 10. Initial system response with (a), (b) a 1000 A (3.6 p.u.) current setpoint, and (c), (d) a 500 A (1.8 p.u.) current setpoint.

For the purpose of our investigation, our scheme will be tailored to a setpoint of 400 A (1.44 p.u.). All four PI controllers were set to user-defined gain input since the proportional gain will be able to vary. This simple control addition is shown in Fig. 11. A delayed RMS current output from the IBR is fed into a switch. The conditional switch will switch from a 'normal' proportional gain value of 4 to a low proportional gain value of 2 where the output current is higher than the current setpoint.

(a)

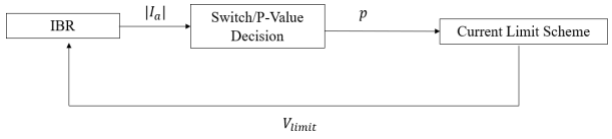

(b)

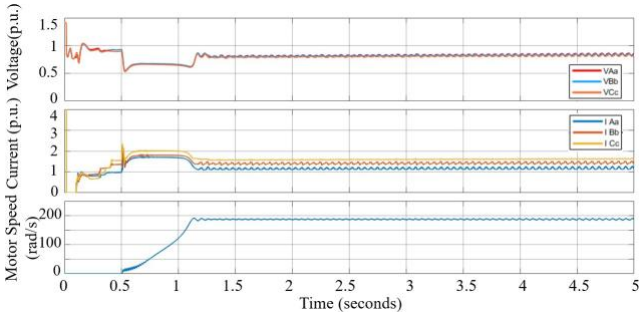

(c)

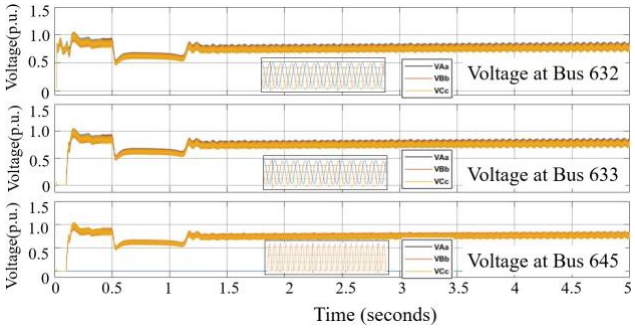

Fig. 11. (a) Flowchart depicting additional proportional gain scheme. (b) and (c) System response with dynamic proportional gain scheme implemented.

The system response, also shown in Fig. 11, does not exceed the 400 A limit (1.44 p.u.). Also note that, although the Fig. 11 dynamic response is stable, the induction motor had a delayed start from previous experiments, and there are severe undervoltage conditions throughout the system. This is another sign of successful performance of the

control scheme, as it shows the scheme's current limiting ability despite the higher system current demand seen in previous experiments. (This stable behavior was verified in an extended 30 second run which is not shown here due to space constraints.).

4. Conclusions and Contributions

There are several significant conclusions that can be drawn from this study in relation to IBR current limit schemes in the blackstart scenarios covered in this paper. Below is a list of such conclusions:

1) Current limit schemes *can* cause instability if not ammended.
2) An automatic voltages setpoint control scheme proves instrumental in combating decreasing voltages as loads are blackstarted in real time.
3) Amending the detailed current scheme to provide a stable response for the IEEE-13 plus induction motor blackstart scenario include (1) Setting the integral gain of the PI controllers of the current limit scheme to zero, and (2) providing a switch that can change proportional gain of the current limit scheme PI controllers.
4) When doing a PI control-based current limit implementation, better performance is found by combining a voltage loop with a current loop, as opposed to using a simplified scheme consisting of a single loop to control current.
5) Implementing a proportional gain switch to the PI controllers of the detailed the current limit scheme proves instrumental in maintaining both current limit capability, as well as stability.

Contributions presented by this paper are the following:

1) This paper provides steps to achieve a successful dynamic response, blackstart, and current limit response from the amended detailed current limit scheme presented. This involves providing novel fixes that made the initially unstable system response to a stable one, which still provides current limitation capability.
2) An enhancement to the detailed current limit scheme, consisting of a proportional gain switch, that switches between two p-gains in real time to achieve a stable response and simultaneously achieve an accurate current limitation.
3) A novel automatic voltage setpoint control scheme enhancement for the IBR was implemented to automatically retain system voltages within 0.95 to 1.05 p.u. as loads are blackstarted.
4) Results from a simplified version of the detailed current control scheme are presented.

Under the assumptions and methodology used, computer implementations of the current limit schemes commonly found in literature can result in unstable results, lack of current clipping, or both. This paper has provided strategies that can remedy these problems when they appear. More sophisticated modeling of the IBR could me implanted; however, since the core fundamentals in the models used in this paper are used the same as any more advanced model, the conclusion that instability *can* occur holds for any IBR model, with any level of sophistication.

Acknowledgements

This work was partially supported by the NSF Grants #OIA-17570207 (NM EPSCoR), HRD-1345232, HRD-1914635, and funding from the Electric Utility Management Program (EUMP) at New Mexico State University.

References

[1] J. Marchgraber and W. Gawlik, "Investigation of black-starting and is- landing capabilities of a battery energy storage system supplying a microgrid consisting of wind turbines, impedance- and motor-loads," MDPI Energies, vol. 13, 5170, October 2020.

[2] J. Himanshu, G. Seo, E. Lockhart, V. Gevorgian, and B. Kroposki, "Black- start of power grids with inverter-based resources," 2020. NREL.

[3] Futurebridge, "Grid-forming inverters: Shaping the future of power distrubution," n.d. Futurebridge Website.

[4] S. Company, "Southern company interconnection requirements of transmission connected inverter-based resources," 2023.

[5] E. Rokrok, T. Qoria, A. Bruyere, B. Francois, and X. Guillaud, "Transient stability assessment and enhancement of grid-forming converters embedding current reference saturation as current limiting strategy," IEEE Transactions on Power Systems, vol. 37, pp. 1519–1531, March 2022.

[6] P. C. Krause, O. Wasynczuk, and S. D. Sudhoff, Analysis of Electric Machinery and Drive Systems. IEEE Press Power engineering Series, Wiley, 2002.

[7] T. Qoria, F. Gruson, F. Colas, K. Xavier, and G. Xavier, "Current limiting algorithms and transient stability analysis of grid-forming vsc's," Elsevier Electric Power Systems Research, vol. 189, December 2020.

[8] G. Fernandez, "Vector current control," n.d. Imperix Website. Accessed Aug 11 2024. https://imperix.com/doc/implementation/vector-current-control

[9] X. Zhao-xia and F. Hong-wei, "Impacts of p-f q-v droop control on microgrids transient stability," 2012. 2012 International Conference on Applied Physics and Industrial Engineering.

[10] N. Mohammed, H. H. Alhelou, and B. Bahrani, Grid-Forming Power Inverters: Control and Applications. CRC Press, 2023.

[11] D. B. Rathnayake, M. Akrami, C. Phurailatpman, S.P. Me, S. Hadavi, G. Jayasinghe, S. Zabihi, and B. Bahrani, "Grid Forming Inverter Modeling, Control, and Applications," IEEE Access, vol. 9, pp. 114781–114807, 2021.

[12] T. Qorai, F. Gruson, F. Colas, X. Guillaud, and M. S. Debry, "Tuning of Cascaded Controllers for Robust Grid-Forming Voltage Source Converter," Power Systems Computation Conference (PSCC), 2018.

[13] A. Alassi, K. Ahmed, A. Egea-Alvarez, and O. Ellabban, "Performance Evaluation of Four Grid-Forming Control Techniques with Soft Black-Start Capabilities." 2020 9th International Conference on Renewable Energy Research and Application (ICRERA), 2020, pp. 221-226.

[14] Grid Forming Inverters: EPRI Tutorial (2023). EPRI, Palo Alto, CA, 2023. 3002028090

[15] D. Brown, "Reactive power-voltage control of inverter based resources,"n.d. Simens Power Technologies International, Consulting Services.

[16] J. D. Glover, M. S. Sarma, and T. J. Overbye, Power System Analysis and Design, Fourth Edition. Thomson Publishing, 2008.

[17] MathWorks, "Thd reduction in ieee-13 bus distribution system," 1994- 2022. Mathworks Website.

[18] The Second Working Group Report, "Special Considerations in Power System Restoration," IEEE Transactions of Power Systems, vol. 9, pp. 15-21, 1992.

[19] P. W. Sauer and M. A. Pai, Power System Dynamics and Stability. Stipes Publishing LLC, 1997.

[20] J. Sawant, G. Seo, and F.Ding, "Resilient Inverter-Driven Blackstart with Collective Parallel Grid-Forming Operation," 2023. NREL.

[21] MathWorks, "Park Transform," 1994- 2024. Mathworks Website..

[22] P. Sushma, B.L Samaga, and K.P Vittal, "DQ Modeling of Induction Motor for Virtual Flux Measurement," 2010. IEEE Xplore.

[23] B. Wen, D. Boroyevich, R. Burgos, P. Mattavelli, and Z. Shen, "DQ Impedance Specification for Balanced Three-Phase AC Distributed Power System," 2015. IEEE Xplore.

[24] R. J. Lee, P Pillay, and R. G. Harley, "D, Q Reference Frames for the Simulation of Induction Motors," Elsevier Electric power Systems Research, vol. 8, pp. 15–26, 1984.

[24] R. Chan, "Grid-connected dc/ac inverter utilizing dq transformation," 2023. Mathworks Website.

[25] I. Geng and A. Hiskens, "Unified grid-forming/following inverter control," IEEE Open Access Journal of Power and Energy, vol. 9, pp. 489–500, 2022.